The effect of pitchfork bifurcations on the spectral statistics of Hamiltonian systems

2007 J. Phys. A: Math. Theor. 40 1525

(http://iopscience.iop.org/1751-8121/40/7/007)

IOP PUBLISHING JOURNAL OF PHYSICS A: MATHEMATICAL AND THEORETICAL

J. Phys. A: Math. Theor. **40** (2007) 1525–1543 doi:10.1088/1751-8113/40/7/007

The effect of pitchfork bifurcations on the spectral statistics of Hamiltonian systems

Marta Gutiérrez[1], **Matthias Brack**[1], **Klaus Richter**[1] **and Ayumu Sugita**[2]

[1] Institute for Theoretical Physics, University of Regensburg, Germany
[2] Osaka City University, Osaka, Japan

Received 24 October 2006, in final form 9 January 2007
Published 30 January 2007
Online at stacks.iop.org/JPhysA/40/1525

Abstract

We present a quantitative semiclassical treatment of the effects of bifurcations on the spectral rigidity and the spectral form factor of a Hamiltonian quantum system defined by two coupled quartic oscillators, which on the classical level exhibits mixed phase space dynamics. We show that the signature of a pitchfork bifurcation is two-fold: beside the known effect of an enhanced periodic orbit contribution due to its peculiar $\hbar$-dependence at the bifurcation, we demonstrate that the orbit pair born *at* the bifurcation gives rise to distinct deviations from universality slightly *above* the bifurcation. This requires a semiclassical treatment beyond the so-called diagonal approximation. Our semiclassical predictions for both the coarse-grained density of states and the spectral rigidity, are in excellent agreement with corresponding quantum-mechanical results.

PACS numbers: 03.65.Sq, 05.45.Mt

1. Introduction

A prominent approach to the quest of 'quantum chaos' involves spectral statistics to characterize the energy-level fluctuations in quantum systems and their interpretation in terms of the dynamics of the corresponding classical system. Classically integrable systems possess uncorrelated energy levels, described by a Poisson distribution [1], while the levels of classically chaotic quantum systems exhibit strong local repulsion. This behaviour is conjectured to be the same as for the eigenvalues of ensembles of random matrices preserving certain general symmetries [2]. Spectral statistics has been investigated, for both integrable [3–5] and chaotic [6–8] systems, employing semiclassical (periodic orbit) approaches, which provide the closest link between classical and quantum properties. For the purely chaotic case, starting with [9], considerable progress has been made recently in understanding energy level correlations semiclassically beyond the so-called diagonal approximation [7] by means of classical correlations between (off-diagonal pairs) of periodic orbits [10].

However, integrability and full chaoticity represent extreme situations which occur rather exceptionally. The most realistic physical situation is that of a system which is neither completely chaotic nor integrable, but whose phase space contains a mixture of stable orbits surrounded by regular islands and chaotic regions. One main feature and structuring element of classical mixed phase space dynamics is the occurrence of bifurcations of periodic orbits upon variations of the energy or other parameters of the Hamiltonian. Moreover bifurcations lead to noticeable effects in the spectral statistics, because in semiclassical trace formulae for the density of states [11, 12], contributions from periodic orbits at a bifurcation exhibit an enhanced weight, compared to that of isolated orbits. This has been demonstrated for the generalized cat map in [13], where the semiclassical signature of a tangent bifurcation was studied on the level of the diagonal approximation.

More generally, in [14, 15] a semiclassical approach was developed for the moments of the level counting function in the presence of several competing generic bifurcations. It was suggested that these moments diverge with a universal 'twinkling exponent' in the semiclassical limit $\hbar \to 0$.

In the present paper we investigate the role of pitchfork bifurcations on the spectral statistics in Hamiltonian systems that are closer to a realistic physical situation than the maps considered so far. We show that bifurcations of short orbits have a considerable effect on the spectral rigidity and the spectral form factor, respectively, even in the almost chaotic case. As a standard system with mixed classical dynamics, we choose the Hamiltonian of two coupled quartic oscillators. Its relevant classical bifurcation characteristics are summarized in section 2. In section 3 we present a detailed semiclassical analysis including a comparison with quantum results for the (smoothed) density of states for different symmetry classes, as a prerequisite for the treatment of spectral correlations in section 4. There we quantitatively analyse deviations of the spectral rigidity from universality employing uniform approximations to derive the semiclassical periodic orbit weights at the bifurcation. We show, in particular, that pairs of orbits (with an action difference smaller than Planck's constant $\hbar$), born at a pitchfork bifurcation, yield important non-diagonal contributions to the spectral form factor and rigidity. The deviations from the quantum chaotic universality are found to be most significant *after*, rather than *at* the bifurcation.

2. The quartic oscillator Hamiltonian

As a representative system we investigate the coupled quartic oscillator (QO) in two dimensions. Its Hamiltonian reads

$$H(x, y, p_x, p_y) = \frac{1}{2}\left(p_x^2 + p_y^2\right) + \frac{1}{4}(x^4 + y^4) + \frac{\alpha}{2}x^2y^2. \tag{1}$$

It has been extensively studied both classically, semiclassically and quantum-mechanically [16–20], as a smooth potential model exhibiting the transition from integrability to chaotic behaviour. Here we summarize the main classical features relevant for the subsequent semiclassical treatment. Since the Hamiltonian (1) is homogeneous, its classical dynamics at different energies E can be related to each other by a simple scaling of coordinates, momenta and time. All actions scale with energy E as $E^{3/4}$ so that the semiclassical limit can be unambiguously taken as $E \to \infty$.

After scaling out the energy the parameter α in equation (1) solely determines the dynamics. The system is integrable for $\alpha = 0$, 1 and 3. For $\alpha = 9$, it is almost completely chaotic: we could not locate any stable periodic orbit with a period up to about four times that of the shortest orbits. For values $\alpha > 9$ the regular fraction of the phase space keeps oscillating with a decreasing amplitude.

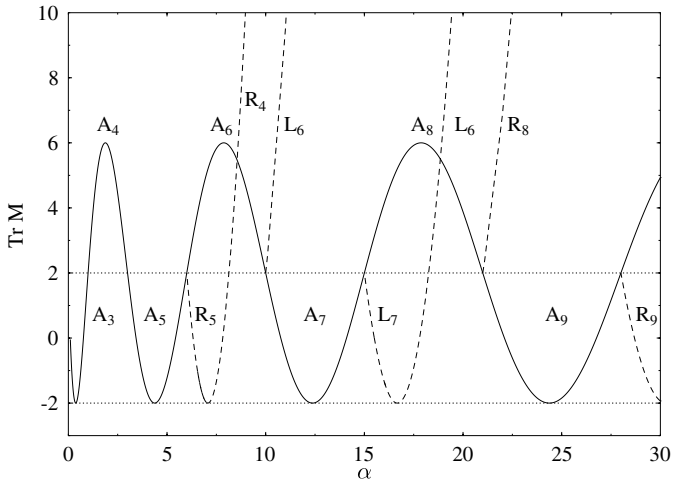

Figure 1. Trace of the stability matrix M as a function of α, equation (1), for the primitive A orbit (solid line) and the new orbits born at its bifurcations (dashed lines) at $\alpha = 6$, 10, 15, 21, and 28. Subscripts denote the Maslov indices σ_j (see section 3).

The QO in equation (1) possesses periodic straight-line librational orbits along both axes which we label by A. They undergo stability oscillations under the variation of α. Infinite cascades of new periodic orbits bifurcate from the A orbits and their repetitions. The motion of the A libration can be given analytically in terms of Lamé functions [18, 19]. The trace of its stability matrix M (see [11, 12] for its definition) as a function of α is known analytically [21]:

$$\mathrm{Tr}\, M(\alpha) = 4\cos\left(\frac{\pi}{2}\sqrt{1+8\alpha}\right) + 2. \tag{2}$$

Isochronous pitchfork bifurcations of the A orbit (which are non-generic due to the discrete symmetries of the system) take place when $\mathrm{Tr}\, M = +2$, i.e., for

$$\alpha = \alpha_n = \tfrac{1}{2}n(n+1), \qquad n = 0, 3, 4, 5, \ldots. \tag{3}$$

(For $\alpha_1 = 1$ and $\alpha_2 = 3$, where the system is integrable, the A orbit is member of a degenerate family and does not bifurcate. See also [18, 19] for more details about the periodic orbits of this system.)

In figure 1 we show $\mathrm{Tr}\, M(\alpha)$ for the primitive A orbit and the new orbits born at its bifurcations at α_n with $n = 3$ to 7. These orbits are alternatively stable or unstable rotational (R_σ) and librational orbits (L_σ) with a classical degeneracy of 2 due to the symmetries (cf [18]). In our numerical case studies below, we shall focus on the bifurcation at $\alpha = \alpha_4 = 10$ where the orbit L_6 is born. Note that at each second bifurcation ($n = 3, 5, \ldots$) a new stable orbit ($\mathrm{R}_5, \mathrm{L}_7, \ldots$) is born, so that stable orbits exist on either side of these bifurcations. At the other bifurcations ($n = 4, 6, \ldots$), on the other hand, the new orbits ($\mathrm{L}_6, \mathrm{R}_8, \ldots$) are unstable, and just before these bifurcations, the A orbit is also unstable. This explains the oscillating regularity of the phase space and the fact that, even in the limit $\alpha \to \infty$, there always exist regions with stable orbits [20]).

The potential in equation (1) is invariant under the symmetry operations that conform the point group symmetry C_{4V}, which has four one-dimensional irreducible representations and one (doubly-degenerate) two-dimensional representation. Due to the C_{4V} symmetry, the full eigenvalue spectrum would not exhibit any universal statistics. For an appropriate study

of the spectral statistics, each symmetry class must therefore be treated separately. We shall study mainly the representation corresponding to eigenfunctions which are symmetric under the operations $x \to -x$, $y \to -y$ and $x \to y$, which we call EES. This representation is easier to handle semiclassically, because all its characters are equal to unity.

For the numerical calculation of the quantum mechanical eigenenergies we follow the procedure outlined in [22]. We diagonalize the Hamiltonian using a basis of symmetry-adapted linear combinations of harmonic oscillator states:

$$|n_x, n_y\rangle_m = \tfrac{1}{\sqrt{2}}(|n_1, n_2\rangle \pm |n_2, n_1\rangle), \tag{4}$$

where the sign and the parity of n_1 and n_2 depends on the representation. Since the independent symmetry-reduced blocks of the Hamiltonian matrix in this basis are banded, we can obtain up to ten thousand well-converged eigenvalues, allowing for significant statistics.

3. Semiclassical density of states for discrete symmetries

Periodic orbit theory yields the semiclassical spectral density as

$$g(E) = \bar{d}(E) + \delta g(E), \tag{5}$$

where the smooth part $\bar{d}(E)$ is given by the (extended) Thomas–Fermi model (cf chapter 4 in [12]), and the oscillating contribution is given by a trace formula which, to leading order in $1/\hbar$, has the following form:

$$\delta g(E) = \frac{1}{\hbar^{\mu+1}} \sum_j A_j(E) \cos\left[\frac{S_j(E)}{\hbar} - \frac{\pi}{2}\sigma_j\right]. \tag{6}$$

The sum is over all periodic orbits j (which form families with degenerate actions in the presence of continuous symmetries). $S_j(E) = \oint_j \mathbf{p} \cdot \mathrm{d}\mathbf{q}$ is the action integral along a periodic orbit and σ_j a geometrical phase factor (usually called Maslov index). The amplitudes $A_j(E)$ and the power of $\hbar$ in equation (6) depend on the presence of continuous symmetries. For systems without continuous symmetries, where all orbits are isolated in phase space, one has $\mu = 0$, and the amplitudes $A_j(E)$ were given by Gutzwiller [23] in terms of their stability matrices $M_j(E)$ and periods $T_j(E) = \mathrm{d}S_j(E)/\mathrm{d}E$. When an isolated periodic orbit undergoes a bifurcation at an energy E_0, its amplitude in the Gutzwiller trace formula diverges and uniform approximations must be developed [24] to obtain a finite $A_j(E_0)$; in this case one finds $0 < \mu \leqslant 1/2$, the precise value of μ depending on the generic type of the bifurcation (cf also [25]). For fully integrable systems, $\mu = f/2$, where f is the degree of degeneracy of the most degenerate orbit families; the amplitudes were derived by Strutinsky and Magner [26] for specific cases and by Berry and Tabor [27] for general integrable systems (cf also section 3.1). For non-integrable systems with continuous symmetries, further results were obtained by Creagh and Littlejohn [28], who also derived a Berry–Tabor-like trace formula for integrable systems.

In the presence of discrete symmetries it is necessary to define partial densities of states corresponding to the subspectra of each irreducible representation of the symmetry group. For systems with isolated orbits, the corresponding symmetry-reduced semiclassical trace formulae have been derived in [29–31]; we shall discuss and use them in section 3.2.

For practical purposes, it is useful to coarse-grain the density of states by convolution with a normalized Gaussian $\exp[-(E/\gamma)^2]/(\sqrt{\pi}\gamma)$. Hence, we replace the quantum density of states $d(E) = \sum_n \delta(E - E_n)$ by the 'coarse-grained' density of states

$$d_\gamma(E) = \frac{1}{\sqrt{\pi}\gamma} \sum_n \exp\left[-\frac{(E - E_n)^2}{\gamma^2}\right], \tag{7}$$

whereby the smoothing width γ defines the energy resolution at which one wishes to study the spectrum. The correspondingly averaged semiclassical level density becomes, to leading order in $\hbar$ (see, e.g., [12]),

$$\delta g_\gamma(E) = \frac{1}{\hbar^{\mu+1}} \sum_j A_j(E) \exp\left[-\left(\frac{\gamma T_j(E)}{2\hbar}\right)^2\right] \cos\left[\frac{S_j(E)}{\hbar} - \frac{\pi}{2}\sigma_j\right]. \quad (8)$$

Hence, long orbits are exponentially suppressed which avoids convergence problems for not too small values of γ.

3.1. Integrable systems

For integrable systems with f degrees of freedom, it is useful to work with action-angle variables $(\mathbf{I}, \phi)$, with each set of actions $\mathbf{I} = \{I_1, \ldots, I_f\}$ defining a phase-space torus [32][3]. The Hamiltonian can be transformed to $H(\mathbf{I}) = E$, and the frequencies $\mathrm{d}\phi/\mathrm{d}t = \omega = \{\omega_1, \ldots, \omega_f\}$ on the torus $\mathbf{I}$ are given by $\omega(\mathbf{I}) = \nabla H(\mathbf{I})$. Assuming smooth boundaries, the Einstein–Brillouin–Keller (EBK) quantization [33]

$$I_j(n_j) = \hbar(n_j + 1/2), \qquad n_j = 0, 1, 2, \ldots, \qquad j = 1, \ldots, f, \quad (9)$$

defines a set of f quantum numbers $\mathbf{n} = (n_1, \ldots, n_f)$. Upon inserting equation (9) into $E = H(\mathbf{I})$, the EBK spectrum reads

$$E^{\mathrm{EBK}}_{\mathbf{n}} = E^{\mathrm{EBK}}_{n_1,\ldots,n_f} = H(I_1(n_1), \ldots, I_f(n_f)). \quad (10)$$

Berry and Tabor [27] started from the density of states in terms of the $E^{\mathrm{EBK}}_{\mathbf{n}}$ and converted it, by means of Poisson summation, into a semiclassical trace formula of the type of equation (6).

The EBK quantization of the integrable QO, equation (1), with $\alpha = 0$ has been performed in [19]; we quote here those results which are relevant for our present application. The EBK spectrum becomes

$$E^{\mathrm{EBK}}_{n_x,n_y} = \frac{1}{4}\left(\frac{3\pi\hbar}{2\mathbf{K}}\right)^{\frac{4}{3}} \left[\left(n_x + \frac{1}{2}\right)^{\frac{4}{3}} + \left(n_y + \frac{1}{2}\right)^{\frac{4}{3}}\right], \qquad (n_x, n_y = 0, 1, 2, \ldots), \quad (11)$$

where $\mathbf{K} = K(\kappa)$ is the complete elliptic integral of first kind with modulus $\kappa = 1/\sqrt{2}$. Since the Hamiltonian (1) is separable for $\alpha = 0$, we can write $E^{\mathrm{EBK}}_{n_x,n_y} = E^{\mathrm{EBK}}_{n_x} + E^{\mathrm{EBK}}_{n_y}$. The separate one-dimensional densities of states,

$$g_j(E) = \sum_{n_j=0}^{\infty} \delta\left(E - E^{\mathrm{EBK}}_{n_j}\right), \qquad (j = x, y) \quad (12)$$

which are identical due to the symmetry, become after Poisson summation

$$g_j(E) = \frac{T_A(E)}{2\pi\hbar} \sum_{k_j=1}^{\infty} (-1)^{k_j} \cos[k_j S_A(E)/\hbar], \qquad (j = x, y) \quad (13)$$

corresponding to the Gutzwiller trace formula for a one-dimensional system. Here

$$S_A(E) = \tfrac{4}{3}\mathbf{K}(4E)^{3/4} \quad (14)$$

is the action of the primitive A orbit and $T_A(E) = \mathrm{d}S_A(E)/\mathrm{d}E$ its period. The total density of states of the full two-dimensional system can then be written as a convolution integral of the one-dimensional densities:

$$g(E) = \int_0^E g_x(E - E') g_y(E')\, \mathrm{d}E'. \quad (15)$$

[3] The action-angle variables do not always exist globally in integrable systems; see, e.g., [32]. For the present QO, however, they are global and given in [19].

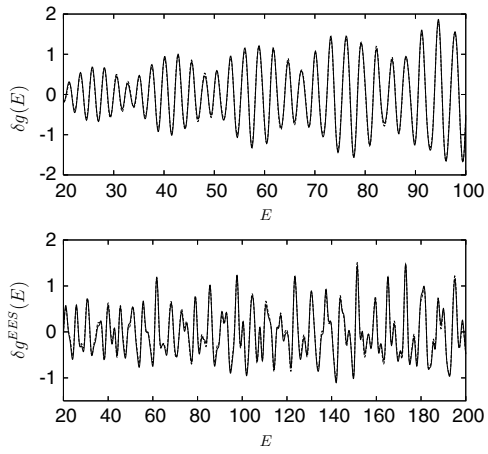

Figure 2. Upper panel: total density of states for $\alpha = 0$ coarse-grained by a Gaussian with width $\gamma = 1$. Lower panel: symmetry-reduced density of states for the representation EES, see the text. Solid line: quantum result, dashed line: semiclassical result, equation (16).

The asymptotic evaluation [34] of this integral in the limit $\hbar \to 0$ yields for the oscillating part

$$\delta g(E) = 2\left(\frac{2\mathbf{K}}{\pi\hbar}\right)^{\frac{3}{2}} (4E)^{\frac{1}{8}} \sum_{k_x=1}^{\infty}\sum_{k_y=1}^{\infty}(-1)^{k_x+k_y}\frac{k_x k_y}{\left(k_x^4+k_y^4\right)^{\frac{5}{8}}}\cos\left[\frac{1}{\hbar}S_{k_x k_y}(E)-\frac{\pi}{4}\right]$$
$$+\frac{(4\mathbf{K})^{\frac{3}{4}}}{(\pi\hbar)^{\frac{5}{4}}}(4E)^{-\frac{1}{16}}\sum_{k=1}^{\infty}(-1)^k\frac{1}{k^{\frac{3}{4}}}\cos\left[\frac{k}{\hbar}S_A(E)-\frac{3\pi}{8}\right]. \tag{16}$$

The double sum in the first line above contains the contributions from the standard stationary-phase evaluation of the integral. It corresponds exactly to the Berry–Tabor trace formula [27], whereby the two numbers k_x, k_y label the rational tori corresponding to the simply degenerate families of periodic orbits with two-dimensional motion. The actions of these rational tori are given by

$$S_{k_x k_y}(E) = S_A(E)\left(k_x^4+k_y^4\right)^{1/4}. \tag{17}$$

The term in the second line of equation (16) arises from the boundaries of the integral (15), corresponding to the A orbits which are one-dimensional librations with all energy in either x ($E' = 0$) or y direction ($E' = E$). Note that the amplitude of this term involves a prefactor $\hbar^{-5/4}$. This is due to the fact that the A orbit undergoes a pitchfork bifurcation at $\alpha = 0$ corresponding to $n = 0$ in equation (3). (The orbits L_3 born at this bifurcation exist only for $\alpha \leqslant 0$.) In [19], identically the same result (16) was obtained, whereby the local uniform approximation [24] for the contribution of the bifurcating A orbit was employed[4].

In the upper panel of figure 2 we compare the semiclassical density of states, equation (16) (dashed line), with the corresponding quantum-mechanical one (solid line), both coarse-grained with a Gaussian average with width $\gamma = 1$. We find perfect agreement up to very high energies.

We now calculate the symmetry-reduced densities of states by restricting ourselves to the subspectra, $E_{\mathbf{n}}^{\mathrm{EBK}}$, of a given irreducible representation. Hereby we can relate the parities of

[4] The parameter a appearing in the corresponding normal form, in the notation of [25] was obtained analytically in [19].

the quantum numbers to the symmetries of the irreducible representations. Thus, we restrict n_x and n_y to be even or odd, according to a given representation. For example, let us take the one-dimensional irreducible representation EES. This corresponds to taking $n_y \leqslant n_x$ with n_x, n_y even. Then the partial density of states can be calculated as a convolution

$$\delta g^{\mathrm{EES}}(E) = \int_0^E g_x^E(E - E') g_y^E(E')\,\mathrm{d}E'$$

of the one-dimensional densities $g_j^E(E)$ defined as in equation (12), except that only the terms with even n_j are included in the sum. The asymptotic evaluation of the convolution integral leads to

$$\delta g^{\mathrm{EES}}(E) = \left(\frac{\mathbf{K}}{\pi\hbar}\right)^{\frac{3}{2}} (4E)^{\frac{1}{8}} \sum_{k_x,k_y=1}^{\infty} \frac{k_x k_y}{\left(k_x^4 + k_y^4\right)^{5/8}} \cos\left[\frac{1}{2\hbar} S_{k_x k_y}(E) - \frac{\pi}{2}(k_x + k_y) - \frac{\pi}{4}\right]$$
$$+ \frac{1}{2^{\frac{3}{4}}} \frac{(\mathbf{K})^{\frac{3}{4}}}{(\pi\hbar)^{\frac{5}{4}}} (4E)^{-\frac{1}{16}} \sum_{k=1}^{\infty} \frac{1}{k^{\frac{3}{4}}} \cos\left[\frac{k}{2\hbar} S_A(E) - \frac{\pi}{2}k - \frac{3\pi}{8}\right]. \tag{18}$$

Again, the first term above corresponds to the Berry–Tabor result for the rational tori, and the second term comes from the bifurcating A orbit.

In the lower panel of figure 2 we compare the semiclassical and quantum-mechanical density of states, $\delta g^{\mathrm{EES}}(E)$, coarse-grained with a Gaussian average with width $\gamma = 1$. Again the agreement is nearly perfect.

3.2. Isolated orbits

The symmetry-reduced densities of states for isolated orbits have been derived in [29, 30] by projecting the semiclassical Green function onto the irreducible representations and reducing the classical dynamics to the fundamental domain which is the smallest part of the phase space which tesselates the whole space under application of the allowed symmetry operations. After this procedure one obtains the reduced density of states in the irreducible representation m,

$$\delta g^m(E) = \frac{d_m}{\hbar} \sum_l \frac{\overline{T}_l}{|K_l|} \sum_r \frac{\chi_m\left(g_l^r\right)}{\left|\overline{M}_l^r - \mathrm{D_l}\right|^{\frac{1}{2}}} \cos\left[\frac{r}{\hbar}\overline{S}_l(E) - \frac{\pi}{2}\overline{\sigma}_{rl}\right]. \tag{19}$$

Here d_m is the dimension and $\chi_m(g)$ the character of the symmetry operator g in the irreducible representation m. The bars in equation (19) indicate that actions, periods, stability matrices and Maslov indices are calculated in the fundamental domain, while g_l^r is the operator that relates the rth repetition of the reduced orbit l with its original lifted into the whole phase space. $|K_l|$ is the order of the group K_l which leaves every point of the orbit l invariant. By the definition of the fundamental domain, this is the identity for orbits that stay in the interior of the fundamental domain, while there can exist more than one operation for orbits that lie on the boundaries. The matrix D_l is block-diagonal in coordinates with blocks given by $\mathrm{d}(gq)/\mathrm{d}q$ with $g \in K$. This matrix is again the identity for interior orbits, but can be different for boundary orbits.

It is usually easier to solve the equations of motion in the whole space than in the fundamental domain, where one has hard-wall reflections. Given the classical quantities for the total space, the task is then to find their reduced counterparts (marked with bars in (19)). Take a Hamiltonian of the form $H(\mathbf{p}, \mathbf{r}) = \mathbf{p}^2/2m + V(\mathbf{r})$ which is invariant under the point-group symmetry G. Suppose that the subgroup H leaves the l orbit invariant (not pointwise), then the l orbit can be divided into $|H|$ copies related by symmetry [35]. There will be $|G|/|H|$ copies of the orbit in the full phase space (if we consider time reversal, then there are

$2|G|/|H|$ copies of orbits without time-reversal symmetry). Therefore the lifted orbit should be equivalent to the $(|H| = r)$th repetition of the reduced orbit (or to the $(|H|/2)$th repetition for time-asymmetric orbits, which become librating orbits in the fundamental domain, and the $(|H|/|K|)$th repetition for boundary orbits). Hence, all the classical quantities should be inter-related as

$$S_l(E) = r\overline{S}_l(E), \qquad T_l(E) = r\overline{T}_l(E), \qquad \sigma_l = r\overline{\sigma}_l, \qquad M_l = \overline{M}_l^r, \tag{20}$$

since they are invariant under point transformations. The only difficulty remains to find out which of the roots of M_l must be taken. E.g., for $|H| = 2$ we have $M_l = \overline{M}_l^2$. Thus, if the eigenvalues of M_l are $\mathrm{e}^{\pm u_l}$, those of $\overline{M}_l$ can be $\pm\,\mathrm{e}^{\pm u_l/2}$. On the other hand, we know that for two-dimensional Hamiltonian systems, hyperbolic orbits always have even Maslov indices, while elliptic and inverse-hyperbolic orbits always have odd Maslov indices [36]. We have observed that this rule can be reversed in the fundamental domain.

This is illustrated in figure 3 for the case of a single reflection symmetry with respect to the x axis. Then the fundamental domain is the upper plane ($y \geqslant 0$). We have calculated the Maslov index $\overline{\sigma}$ using the method of Creagh *et al* [37] (as explained in [12], appendix D) and verified that it is, indeed, either the same as for the lifted orbit for orbits without this symmetry, or half of it for orbits with reflection symmetry. However, the sign of the eigenvalues did not follow Sugita's rule [36]. This rule can, however, be applied to $\overline{\sigma} - \mathrm{mod}(R, 2)$, where R indicates the number of hard-wall reflections at the boundaries of the fundamental domain. Thus, if this number is odd, the rule is reversed.

We have calculated the reduced density of states (19) for the representation EES in the QO at $\alpha = 9$. The result is shown in figure 4 for Gaussian smoothing with width $\gamma = 4$. A considerable agreement between the semiclassical (dotted line) and the quantum-mechanical result (solid line) is achieved.

4. Spectral rigidity

To study the effect of pitchfork bifurcations on the spectral statistics we consider the spectral rigidity or stiffness, Δ [38]. It is defined as the local average of the mean-square deviation of the staircase function $N(E)$ from its best-fit straight line over an energy range corresponding to L states with mean level spacing $\bar{d}$:

$$\Delta(L) = \left\langle \min_{A,B} \frac{\bar{d}}{L} \int_{-L/2\bar{d}}^{L/2\bar{d}} \mathrm{d}\epsilon [N(E+\epsilon) - A - B\epsilon]^2 \right\rangle. \tag{21}$$

The quantity $\Delta(L)$ measures spectral correlations over energy distances of order L. For an uncorrelated Poisson spectrum the universal prediction is

$$\Delta^{\mathrm{Poisson}}(L) = L/15, \tag{22}$$

while for a chaotic system it is approximately given by

$$\Delta^{\mathrm{RMT}}(L) = \frac{\beta}{2\pi^2} \log L - D, \tag{23}$$

where D is a constant, $\beta = 1$ for systems without time reversal symmetry (GUE statistics) and $\beta = 2$ for systems with time reversal symmetry (GOE statistics). This universal behaviour has been observed up to correlation lengths $L < L_{\max} = 2\pi\hbar\bar{d}/T_{\min}$, where $T_{\min}$ is the period of the shortest orbit. In figure 5 we show the numerical results for the quartic oscillator in the integrable and almost chaotic regime, compared with the corresponding predictions, equations (22), (23). The L range, in which the numerical data coincide with the universal predictions, increases with increasing energy, i.e., by approaching the semiclassical limit.

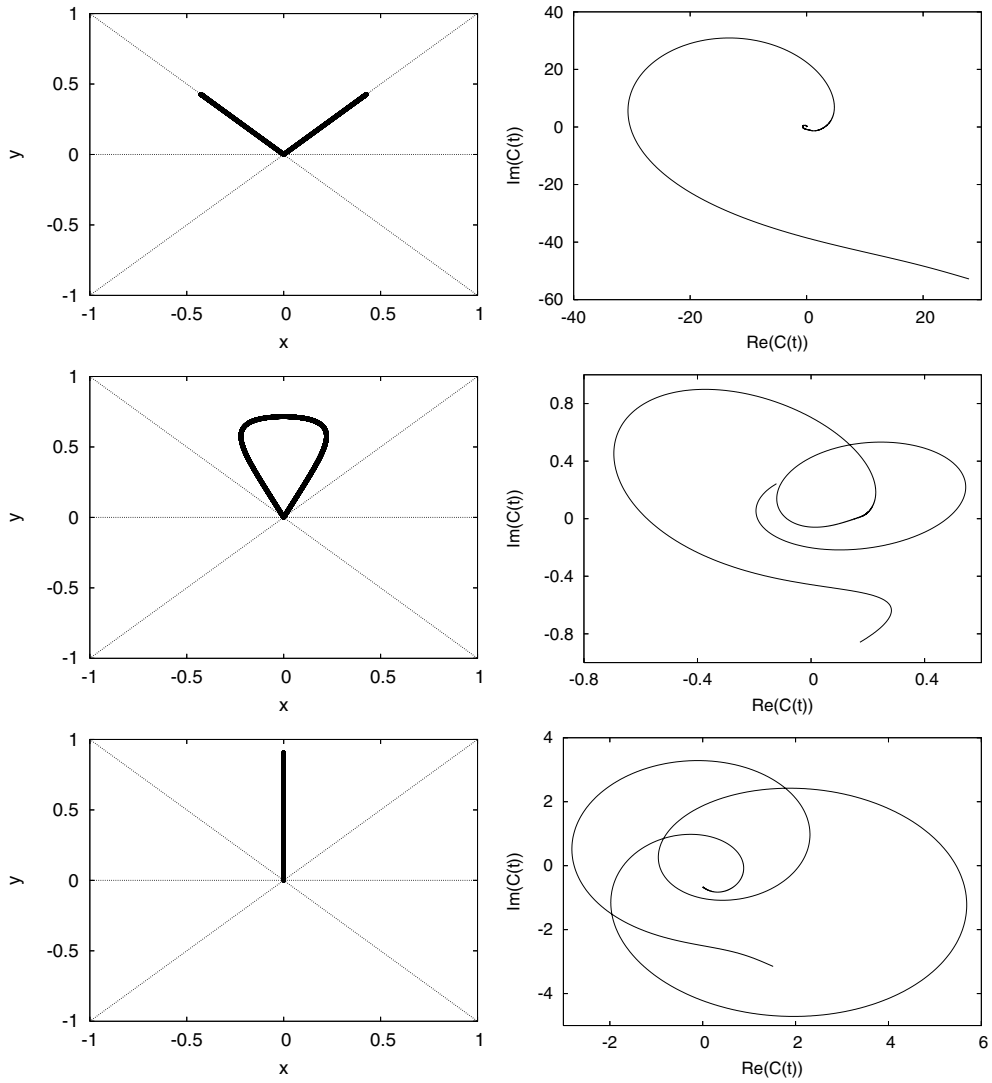

Figure 3. Calculation of Maslov indices for some reduced orbits of the QO at $\alpha = 9$, considering only the reflexion symmetry at the x axis. *Left panels:* reduced orbits in (x, y) plane. *Right panels:* evaluation of the Maslov index $\overline{\sigma}$ which corresponds to the winding number of the complex number $C(t)$ over one period (cf [37]). *Top panels:* librational orbit B_2 along the diagonal. Here the length of the reduced orbit is the same as that of the lifted orbit, and their Maslov indices are equal. *Centre panels:* orbit R_4. Here the reduced orbit is half of the lifted orbit and its Maslov index is $\overline{\sigma} = 2$ (i.e., half of the total σ) but Tr M is negative in spite of the even Maslov index. *Bottom panels:* orbit A_6. The reduced orbit is again half of the total orbit, and so is the Maslov index. But Tr M is positive in spite of the odd Maslov index.

For a mixed system it was conjectured that the statistics will be a superposition of Poisson and random matrix contributions [39, 40], parameterized as

$$\Delta(L) \approx \Delta^{\text{Poisson}}((1-q)L) + \Delta^{\text{RMT}}(qL), \tag{24}$$

where q is the irregularity fraction of the system (i.e., the fraction of the phase space corresponding to the chaotic sea). Since both statistics are monotonously increasing functions, we expect that the more regular the system is, the larger is the rigidity.

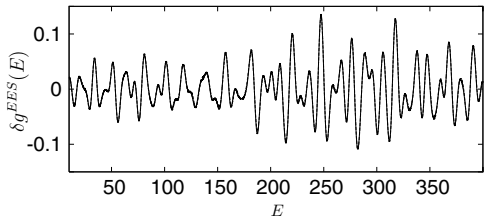

Figure 4. Reduced density of states for the representation EES in the QO at $\alpha = 9$ after Gaussian averaging with width $\gamma = 4$. The solid line shows the quantum result and the dotted line the semiclassical result using equation (19).

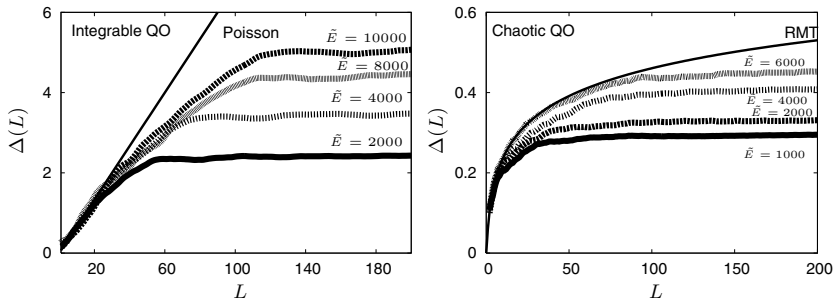

Figure 5. Rigidity for $\alpha = 0$ (integrable case) and $\alpha = 9$ (almost chaotic case). With increasing (unfolded) energy $\tilde{E}$ the numerical data converge to the universal Poisson (left panel) and random matrix predictions (right panel) marked as full lines.

4.1. Semiclassical theory for the rigidity

The semiclassical theory for the rigidity was developed in [7], for the two limiting cases of complete chaoticity and full regularity (integrability). The procedure is the following: by energy integration of the density of states, equation (6), one obtains an expression for the number of states. By inserting this expression into the definition of the rigidity one finds

$$\Delta(L) = \frac{1}{2\hbar^{2\mu}} \left\langle \sum_j \sum_k \frac{A_j A_k}{T_j T_k} \cos\left[\frac{1}{\hbar}(S_j - S_k) + \frac{\pi}{2}(\sigma_j - \sigma_k)\right] G(y_j, y_k) \right\rangle, \tag{25}$$

where $T_j = \mathrm{d}S_j/\mathrm{d}E$ are the periods,

$$y_j = \frac{LT_j}{2\hbar\bar{d}} = \pi \frac{L}{L_{\max}} \frac{T_j}{T_{\min}}, \tag{26}$$

and

$$G(x, y) = F(x - y) - F(x)F(y) - 3F'(x)F'(y), \tag{27}$$

$$F(x) = \frac{1}{x} \sin x = j_0(x). \tag{28}$$

The main contributions come from pairs of orbits whose action difference is smaller than $\hbar$, so that y_j can be chosen to be equal to y_k in the argument of G:

$$\Delta(L) = \frac{1}{2\hbar^{2\mu}} \left\langle \sum_j \sum_k \frac{A_j A_k}{T_j T_k} \exp\left[\frac{i}{\hbar}(S_j - S_k) + \frac{\pi}{2}(\sigma_j - \sigma_k)\right] g(\bar{y}_{j,k}) \right\rangle, \tag{29}$$

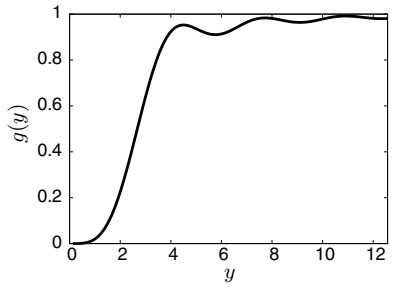

Figure 6. Window function $g(y)$, see the text.

where $\bar{y}_{jk} = \frac{1}{2}(y_j + y_k)$ and $g(x) = G(x, x)$. The function $g(y)$ (see figure 6) selects the orbits that contribute to the double sum. If $L \ll L_{\max}$ then $g(y)$ is almost unity only for long orbits, while for $L > L_{\max}$ the function is almost unity for all y, and the most important contributions to $\Delta(L)$ come from short orbits due to the factor $1/T^2$. Since we are interested in studying the effects of a bifurcation of one of the shortest orbits, we are going to concentrate on the saturation behaviour, which corresponds basically to the first moment of the staircase function.

The rigidity can be written in terms of the spectral form factor $K(\tau)$ (the Fourier transform of the autocorrelation function) as

$$\Delta(L) = \frac{1}{2\pi^2} \int \frac{K(\tau)}{\tau^2} g(\pi L \tau)\, \mathrm{d}\tau, \tag{30}$$

with $\tau = T/2\pi\hbar\bar{d}$ and $K(\tau) = \left\langle \frac{1}{\bar{d}} \int_{-\infty}^{\infty} \langle d(E+\omega/2) d(E-\omega/2) \rangle\, \mathrm{e}^{-2\pi \mathrm{i}\omega\tau\bar{d}}\, \mathrm{d}\omega \right\rangle_{\Delta\tau}$. A local time average $\Delta\tau$ has to be performed in order to obtain a self-averaging form factor.

The corresponding semiclassical expression for the form factor, analogous to equation (29), is

$$K(\tau, E) = \frac{1}{\hbar^{2\mu}} \left\langle \sum_{j,k} \frac{A_j A_k}{T_H^2} \cos\left[\frac{1}{\hbar}(S_j - S_k) + \frac{\pi}{2}(\sigma_j - \sigma_k)\right] \delta_{\Delta\tau}\left(\tau - \frac{\bar{T}_{jk}}{T_H}\right) \right\rangle_{\Delta E}, \tag{31}$$

where $\bar{T}_{jk} = \frac{1}{2}(T_j + T_k)$. The width of the delta-function is due to the time average $\Delta\tau$.

As expressed in equations (29) and (31), the rigidity and the spectral form factor are determined by a double sum over pairs of periodic orbits. The semiclassical limit $\hbar \to 0$ means that the typical classical actions of these paths are very large compared with $\hbar$, so that the energy average will strongly suppress the contributions of most pairs of orbits. The first approximation is to consider that only orbits paired with themselves ($j = i$) or with their time-reserved partners ($j = \bar{i}$) give a contribution, which is known as the 'diagonal approximation' [7].

For the QO at $\alpha = 0$, the tori amplitudes $A_{kx,ky}$ are given by

$$A_{kx,ky} = \left(\frac{\mathbf{K}}{\pi}\right)^{3/2} (4E)^{1/8} \frac{k_x k_y}{(k_x + k_y)^{5/8}} \tag{32}$$

for the irreducible representation EES. For integrable systems the contribution of the non-diagonal terms $j \neq k$ in the sum (25) will vanish after averaging owing to destructive interference. For this system, due to the degeneracy in the actions, the orbits that contribute to the double sum are those that satisfy $n_x^4 + n_y^4 = n_x'^4 + n_y'^4$. Inserting the amplitudes for the

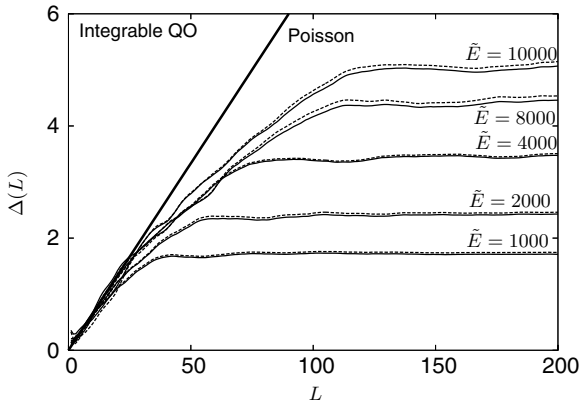

Figure 7. Semiclassical (dashed lines) and quantum results (solid lines) for the spectral rigidity $\Delta(L)$ for different values of $\tilde{E}$.

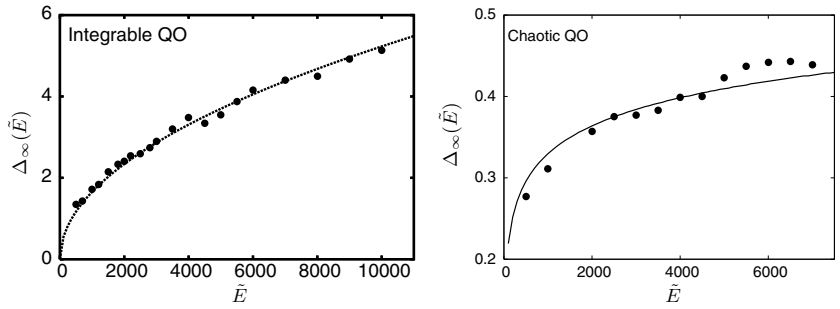

Figure 8. Saturation value Δ_∞ plotted versus unfolded energy $\tilde{E}$. The dots mark the quantum results. Left panel: integrable case ($\alpha = 0$); the solid line shows the semiclassical prediction. Right panel: almost chaotic case ($\alpha = 9$). Here the solid line represents the GOE prediction.

tori and summing only over terms with the same actions we have

$$\Delta(L) = \frac{(4E)^{3/4}}{2^4\pi^3\hbar\mathbf{K}} \sum_{k_x,k_y=1}^{\infty} \frac{k_x k_y}{l_k^7} g\left(\bar{y}_{k_x,k_y}\right) \sum_{n_x,n_y=1}^{\infty} n_x n_y \delta_{l_k - l_n}, \tag{33}$$

where $l_k = \left(k_x^4 + k_y^4\right)^{1/4}$, $l_n = \left(n_x^4 + n_y^4\right)^{1/4}$, and δ is the Kronecker delta.

With this expression, we can reproduce very well the statistics semiclassically, as is shown in figure 7.

We have neglected here the contribution of the A orbit which undergoes a pitchfork bifurcation. We have checked that its contribution is negligible, since its amplitude in the PO expansion goes like $\hbar^{-5/4}$ (a power one quarter larger than an isolated orbit) compared with that ($\hbar^{-3/2}$) of the tori. For the saturation we can take $g\left(y_{k_x,k_y}\right) = 1$. Then the energy dependence of the saturation value Δ_∞ goes like $E^{3/4}$, as seen from equation (33).

In the left panel of figure 8 we depict the saturation value obtained from the quantum spectrum (dots), which is well reproduced by the semiclassical prediction (solid line). For the chaotic case, RMT gives a saturation value Δ_∞ that behaves as $\log(1/\hbar)$ which is obtained by replacing the form factor by its GOE prediction in equation (30). Though the exact saturation

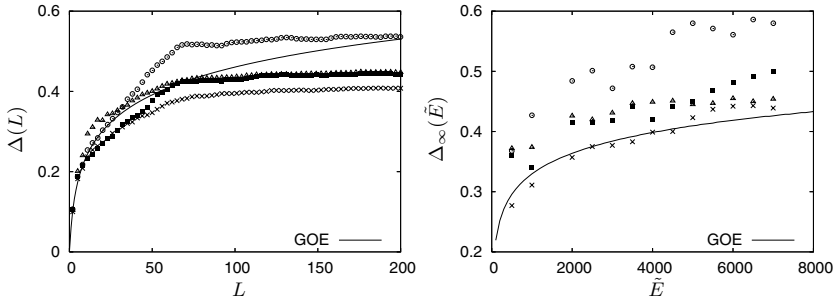

Figure 9. Left panel: spectral rigidity for $\alpha = 9$ (crosses), $\alpha = \alpha_4 = 10$ (filled squares), $\alpha = 10.5$ (circles), and $\alpha = 11$ (triangles) for $\tilde{E} = 4000$. Right panel: saturation value Δ_∞ versus $\tilde{E}$ before and after the bifurcation at $\alpha_4 = 10$. Although the phase space is barely affected, the saturation at $\alpha = 10.5$ is much larger than the saturation at $\alpha = 11$.

value is not universal, since it depends on the lower integration limit $\tau_{\min}$, its $\hbar$ dependence is. In the right panel of figure 8 we compare the quantum result with the GOE prediction evaluated for our value of $T_{\min}$ for $\alpha = 9$.

4.2. Bifurcation effects in the rigidity

It has been discussed in [13] that additional contributions to the long-range spectral correlations may arise from bifurcations of periodic orbits, and that this effect can be reproduced semiclassically. The authors of [13] investigated the cat map at a tangent bifurcation, and found that the number variance of the counting function shows a 'lift off' reaching a much higher value than in the normal chaotic situation. We report here similar findings for the rigidity of the QO Hamiltonian for values of α near the pitchfork bifurcations of the A orbit at α_n. Moreover, we find that the increase of the saturation value Δ_∞ becomes even larger slightly above the bifurcations. This is illustrated in figure 9. In the left panel we show the rigidity $\Delta(L)$ for four values of α around $\alpha = \alpha_4 = 10$ where such a bifurcation occurs. The rigidity at $\alpha_4 = 10$ exhibits a slightly larger saturation than at $\alpha = 9$ ('lift off'). However, the increase is even much more noticeable at $\alpha = 10.5$. Then the saturation goes down again for $\alpha = 11$, even though the system is more regular than at $\alpha = 10.5$.[5]

The energy dependence of Δ_∞ is shown in the right panel of figure 9. We see that this effect exists over a large region of energies. As depicted in figure 11 the phase space looks completely chaotic at the bifurcation at $\alpha = 10$; without knowledge of the bifurcation one would expect an almost universal behaviour. Above the bifurcation, a tiny regular island is seen at the centre, which arises from orbit A_7 that became stable. The island is slightly larger at $\alpha = 11$ than at $\alpha = 10.5$ (see figure 11).

Equivalently, in figure 10 we show the effect in the spectral form factor. In the left panel we show $K(\tau)$ at $\alpha = 9, 10$ and 11. The results are consistent with the GOE prediction for almost all times, but we see a very large peak at a time that corresponds to the period of the libration orbit, τ_A. This is consistent with the results of [13]. However, the enhancement is even more noticeable at $\alpha = 10.5$ (right panel).

The exact calculation of the semiclassical rigidity for the QO in the chaotic regime is numerically impossible, since this would require an infinite number of periodic orbits, and

[5] To verify this, we calculated the chaoticity fraction q by fitting the nearest-neighbour spacing distribution to the interpolation formula given in [39].

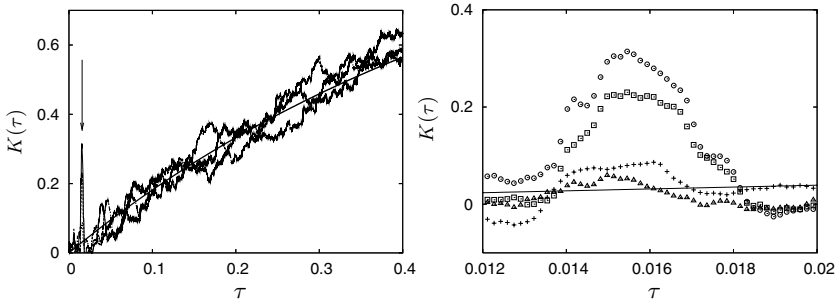

Figure 10. *Left panel:* form factor at $\alpha = 9$, 10 and 10.5 compared with RMT (line). Note the strong peak at $\tau = \tau_A \simeq 0.015$ (indicated by an arrow) coming from the bifurcating orbit. *Right panel:* form factor at $\alpha = 9$ (crosses), $\alpha = 10$ (squares), $\alpha = 10.5$ (circles), and $\alpha = 11$ (triangles) in a zoomed region around $\tau \simeq \tau_A$. For $\alpha = 10.5$: the amplitude of the peak is clearly larger than at the bifurcation.

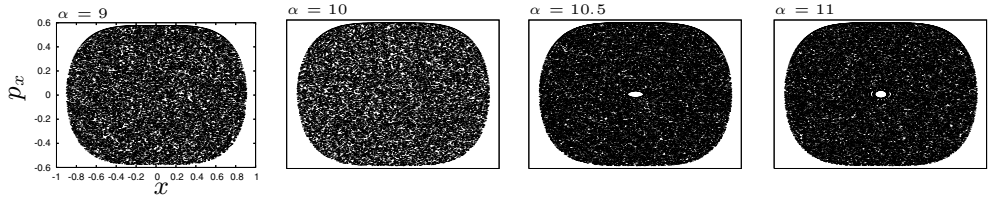

Figure 11. Poincaré surfaces of section for the QO near α_4. At $\alpha = 9$ and at the bifurcation point $\alpha = 10$ the phase space looks completely chaotic. A new stable island appears at $\alpha = 10.5$, which is slightly larger at $\alpha = 11$.

there is no analytical way to calculate them. To reproduce the quantum result semiclassically, we calculate the coarse-grained reduced density of states, defined analogously to equation (8) by

$$\delta g_\gamma^m(E) = \frac{d_m}{\hbar} \sum_l \frac{\overline{T}_l}{|K_l|} \mathrm{e}^{-(\gamma \overline{T}_l/2)^2} \sum_r \frac{\chi_m(g_l^r)}{\left|\overline{M}_l^r - \mathrm{D_l}\right|^{\frac{1}{2}}} \cos\left[\frac{r}{\hbar}\overline{S}_l(E) - \frac{\pi}{2}\overline{\sigma}_{rl}\right]. \tag{34}$$

The longer orbits will be exponentially suppressed assuring convergence, but, at the same time, affecting the universality. However, for the study of the saturation properties of $\Delta(L)$ as a probe for bifurcation effects, the information of the shorter orbits should be sufficient.

Consistently we also coarse-grain the quantum stair-case function, defining

$$N_\gamma(E) = \frac{1}{2} \sum_n \left[1 - \mathrm{erf}\left(\frac{E_n - E}{\gamma}\right)\right]. \tag{35}$$

Inserting $N_\gamma(E)$ into equation (21), we obtain a 'smoothed' rigidity Δ_γ of the coarse-grained density of states. We find that even for relatively large values of γ, the bifurcation effects described above are still clearly visible, as shown in figure 12.

We are now equipped to calculate the saturation property of the smooth rigidity $\Delta_\gamma(L)$ semiclassically, taking into account the bifurcation of the A orbit at $\alpha_4 = 10$. Its contribution to the total density of states, together with that of the L_6 orbits born at the bifurcation, to the total density of states is given in the 'global' uniform approximation of [25] (with $\sigma = +1, a < 0$,

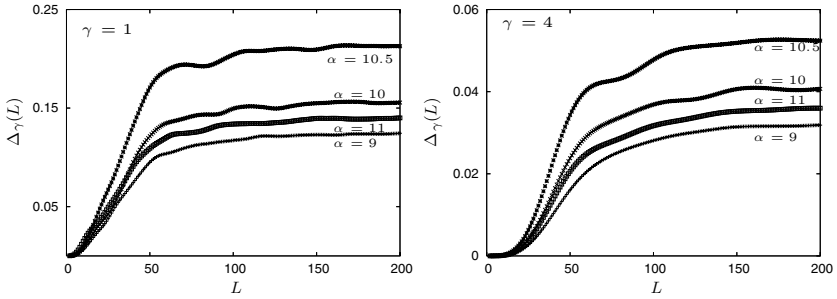

Figure 12. Same as figure 9, but after coarse-graining the reduced quantum spectrum by a Gaussian smoothing with width $\gamma = 1$ (left) and $\gamma = 4$ (right).

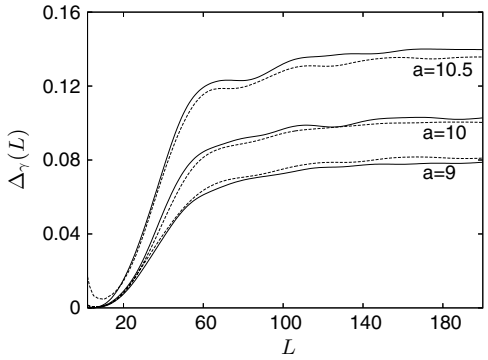

Figure 13. Smoothed rigidity for $\alpha = 9, \alpha = \alpha_4 = 10$ and $\alpha = 10.5$, obtained for $\gamma = 2$. The solid (dashed) curves represent the quantum mechanical (semiclassical) results.

$\sigma_1 = -1$ and $\nu = \sigma_{A_6,r} = 6r$ for the present case). It reads

$$\delta g^{un}_{A+L}(E) = \mathrm{Re}\frac{1}{\pi\hbar}\left|\frac{\pi\Delta S}{2\hbar}\right|^{1/2}\exp\left(\frac{\mathrm{i}}{\hbar}\overline{S} - \mathrm{i}3r\pi - \mathrm{i}\frac{\pi}{4}\right)$$
$$\times\left\{\overline{A}\left[\sigma_2 J_{1/4}\left(\frac{|\Delta S|}{\hbar}\right)\mathrm{e}^{-\mathrm{i}\frac{\pi}{8}} + J_{-1/4}\left(\frac{|\Delta S|}{\hbar}\right)\mathrm{e}^{\mathrm{i}\frac{\pi}{8}}\right]\right.$$
$$\left.+\,\Delta A\left[J_{3/4}\left(\frac{|\Delta S|}{\hbar}\right)\mathrm{e}^{-3\mathrm{i}\frac{\pi}{8}} + \sigma_2 J_{-3/4}\left(\frac{|\Delta S|}{\hbar}\right)\mathrm{e}^{3\mathrm{i}\frac{\pi}{8}}\right]\right\}. \tag{36}$$

Here $\Delta A = A_L/2 - A_A/\sqrt{2}$, $\overline{A} = A_L/2 + A_A/\sqrt{2}$, $\overline{S} = (S_L + S_A)/2$ and $\Delta S = (S_L - S_A)/2$, where $A_j(E)$ and $S_j(E)$ are the Gutzwiller amplitudes and actions of the isolated A and L orbits, respectively, away from the bifurcation, r is their repetition number, and $\sigma_2 = \mathrm{sign}(\alpha - \alpha_4)$. At the bifurcation ($\alpha = \alpha_4 = 10$), the local uniform approximation becomes

$$\delta g^{\mathrm{loc}}_{A+L}(E) = \frac{T_A\Gamma(\frac{1}{4})}{2\pi\sqrt{2\pi}\hbar^{5/4}|a|^{1/4}r^{3/4}}\cos\left[\frac{S_A}{\hbar} - 3r\pi + \frac{\pi}{8}\right]. \tag{37}$$

Here $T_A(E)$ is the period of the primitive A orbit, and a is a normal form parameter which we determined numerically from the local expansion given in equation (41) below (cf also [19, 25]).

In this way we can reproduce the quantum mechanical results near the bifurcation semiclassically, as demonstrated in figure 13. Further analysis showed that amplitudes and

actions of most of the orbits do barely change, and the higher saturation for the smooth rigidity was mainly caused by the bifurcation.

Considering the rigidity without smoothing, we now assume that the contribution of the long orbits corresponds to and can be replaced by the universal RMT prediction, so that the differences in the saturations arise basically from the A and L orbits. Hence, we approximate the saturation value of Δ by

$$\begin{aligned}\Delta_\infty(E) &\simeq \Delta_\infty^{\mathrm{GOE}} + \Delta_\infty^{A,L} \\ &\simeq \Delta^{\mathrm{GOE}} + \frac{1}{2}\left\langle \sum_{j,k=A,L} \frac{A_j A_k}{T_j T_k} \cos\left(\frac{S_j - S_k}{\hbar}\right)\right\rangle. \end{aligned} \tag{38}$$

At the bifurcation, the second term corresponds to the diagonal contribution of (37), so that

$$\Delta_\infty^{A,L} = \frac{\Gamma^2(1/4)}{8\pi^3|a|^{1/2}\hbar^{1/2}}, \tag{39}$$

and Δ_∞ behaves like

$$\Delta_\infty \propto \log(1/\hbar) + \frac{1}{\hbar^{1/2}}. \tag{40}$$

In the neighbourhood of the bifurcation, i.e., when the action difference $|\Delta S|$ is smaller than $\hbar$, we can expand the actions and amplitudes around $\alpha = \alpha_4$ (cf [25]):

$$\Delta S = \frac{S_A - S_L}{2} = \frac{\epsilon^2}{4a} + O(\epsilon^3), \tag{41}$$

$$A_A = \frac{T_A}{\sqrt{2\epsilon}}, \qquad A_L = \frac{T_A}{\sqrt{\epsilon}}\left[1 + O(\epsilon)\right], \tag{42}$$

where $\epsilon = c(\alpha - \alpha_4)$. Up to first order in ϵ this yields

$$\delta g_{A+L}^{un}(E) \approx \frac{T_A}{\pi\sqrt{2\pi\hbar}} \operatorname{Re} \mathrm{e}^{\mathrm{i}\bar{S}/\hbar - \mathrm{i}3k\pi - \mathrm{i}\pi/4}\left[\frac{\sigma_2\Gamma(3/4)}{|a\hbar|^{3/4}}\epsilon\, \mathrm{e}^{-\mathrm{i}\pi/8} + \frac{\Gamma(1/4)}{2|a\hbar|^{1/4}}\, \mathrm{e}^{\mathrm{i}\pi/8}\right]. \tag{43}$$

Inserting this into the saturation value of the rigidity we obtain

$$\Delta_\infty^{A,L} \approx \frac{\Gamma^2(1/4)}{8\pi^3|a|^{1/2}\hbar^{1/2}} + \epsilon\frac{1}{2\pi^2|a|\hbar} + \epsilon^2\frac{\Gamma^2(3/4)}{2\pi^3|a|^{3/2}\hbar^{3/2}}. \tag{44}$$

Equivalent results are obtained for the form factor considering only the contributions of the orbits involved in the bifurcation.

In figure 14 we show the quantum results for Δ_∞ versus energy $\tilde{E}$ and for the form factor $K(\tau)$ near τ_{A}, for the three values $\alpha = 9$, 10 and 10.5 (as crosses, squares and circles, respectively). The solid line gives the universal GOE prediction, i.e., the first term in (40). It agrees well with the quantum result at $\alpha = 9$, in line with the near chaoticity of the system below the bifurcation. The dashed and dotted lines show the prediction (44), which includes the bifurcating orbits A and L in the uniform approximation, and coincide well with the quantum results at and above the bifurcation. At the bifurcation ($\alpha = \alpha_4 = 10$) where $\epsilon = 0$, equation (44) is consistent with the diagonal approximation for the bifurcating orbits and thus the same as that used in [13].

Figure 14 moreover shows that slightly above the bifurcation, i.e. at $\alpha = 10.5$, the additional terms in equation (44), playing a role for $\epsilon \neq 0$, give a noticeable contribution, as seen by the dashed line. The main contribution comes from the term linear in ϵ which is the

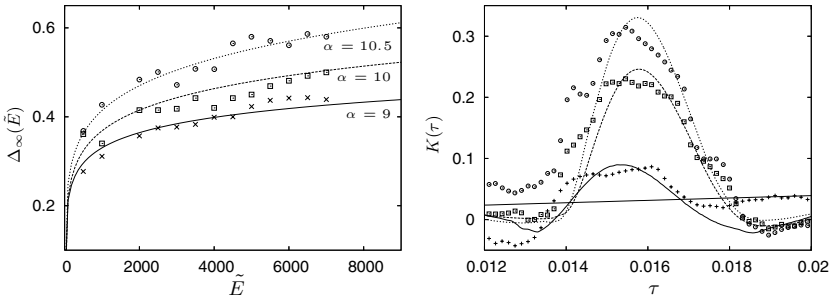

Figure 14. *Left*: saturation as a function of the energy. *Right*: form factor near τ_A. Crosses, squares and circles mark quantum-mechanical results for $\alpha = 9$, 10 and 10.5, respectively. Bold line: GOE result, dashed and dotted lines: equation (44).

non-diagonal contribution of the pairs of separate orbits A and L above the bifurcation. To see this, we evaluate their non-diagonal contribution in the Gutzwiller approximation for isolated orbits, which would become

$$\Delta_{\infty(\mathrm{Gutz})}^{A.L(\mathrm{non\text{-}diag})} = 2\frac{A_L A_A}{\pi^2 T_A^2}\left\langle \sin\left(\frac{\Delta S}{\hbar}\right)\right\rangle \approx \frac{\sqrt{2}}{\pi^2\epsilon}\frac{\Delta S}{\hbar} = \frac{\epsilon}{2\sqrt{2}\pi^2|a|\hbar}. \tag{45}$$

(Although the diagonal contribution diverges at the bifurcation, the non-diagonal contribution stays finite there.) The additional factor $1/\sqrt{2}$, compared to the last term in equation (44), is due to the fact that the Gutzwiller approximation is not yet valid in this vicinity of the bifurcation (in particular, the difference in Maslov indices is different from the value 1 reached only far from the bifurcation where $\Delta S \gg \hbar$ and hence $\epsilon \gg 1$).

We see therefore that the non-diagonal contribution of the bifurcating orbits to the saturation value Δ_∞ is non-negligible in a neighbourhood above the bifurcation. Note that the value of Δ_∞ is slightly enhanced also by the fact that the particular combination of Bessel functions in the uniform approximation (36) can be expressed by an Airy function (and its derivative, cf [25]), which has its maximum slightly above the bifurcation. This effect is, however, not sufficient to explain the enhancement of Δ_∞ found in our results, so that we can argue that the non-diagonal contribution is substantial.

It is important to mention that this non-diagonal contribution exists as long as $\hbar$ remains finite. In the strict semiclassical limit $\hbar \to 0$, the global uniform approximation (36) merges into the Gutzwiller trace formula for non-zero ΔS, and $\sin(\Delta S/\hbar)$ oscillates very fast, so that after the coarse-graining, the non-diagonal contribution will tend to zero. This is expected, since in the semiclassical approximation for mixed systems (equation (24)), periodic orbits with different stability give rise to independent statistics.

5. Conclusions

In this case study we worked out for the quartic oscillator how (pitchfork) bifurcations affect the density of states and thereby further measures of spectral correlations. This requires, at a first stage, detailed knowledge about the classical bifurcation scenario in that system. At a second stage, we performed a comprehensive semiclassical calculation for the density of states invoking uniform approximations for the bifurcating orbits involved. All features of the coarse-grained quantum density of states are adequately, and to high precision (mean level spacing), semiclassically reproduced, which is not evident in such a system with mixed phase space dynamics. Our semiclassical evaluation of the spectral rigidity close to the

bifurcation shows strong deviations from the RMT behaviour, even though the phase space is predominantly chaotic and the bifurcation-affected phase space region appears negligible. This confirms that spectral statistics is rather susceptible with respect to bifurcation effects. Moreover we could unreveal the role of orbit pairs born at the bifurcation which prevail with near-degenerate actions for larger control parameter regimes and strongly affect the spectral statistics. Such orbit pairs are obviously classically correlated and require a treatment beyond the diagonal approximation.

This analysis moreover implies that in a comprehensive semiclassical approach to spectral correlations in mixed systems, which still remains as a challenge, off-diagonal contributions in the occurring multiple sums over periodic orbits should be considered, analogously to the purely hyperbolic case.

Further open questions not answered in the present work include a corresponding analysis of how eigenstates are affected at a bifurcation. Finally, studies of bifurcation signatures in other observables such as quantum transport are still rare [15] and remain to be explored.

Acknowledgments

We thank S Creagh, J Keating, P Schlagheck and M Sieber for useful discussions and are grateful to K Jänich for his assistance in evaluating the boundary term in equation (16). The numerical determination of the periodic orbits and their stabilities was done with the program developed by Ch. Amann in [42]. We acknowledge financial support of the *Deutsche Forschungsgemeinschaft* (GRK 638). We are grateful to B Zhilinskii for fruitful criticism and to our anonymous referees for a number of valuable corrections,

References

[1] Berry M V and Tabor M 1977 *Proc. R. Soc.* A **356** 375
[2] Bohigas O, Giannoni M J and Schmit C 1984 *Phys. Rev. Lett.* **52** 1
[3] Casati G and Chirikov B V 1985 *Phys. Rev. Lett.* **54** 1350
[4] Robnik M and Veble G 1998 *J. Phys. A: Math. Gen.* **31** 4669
[5] Bogomolny E 2000 *Nonlinearity* **13** 947
[6] Hannay J and de Almeida A M Ozorio 1984 *J. Phys. A: Math. Gen.* **17** 3429
[7] Berry M V 1985 *Proc. R. Soc.* A **400** 229
[8] Argaman N, Dittes F M, Doron E, Keating J P, Kitaev A Yu, Sieber M and Smilansky U 1993 *Phys. Rev. Lett.* **71** 4326
[9] Sieber M and Richter K 2001 *Phys. Scr.* T **90** 128
Sieber M 2002 *J. Phys. A: Math. Gen.* **35** L616
[10] Berkolaiko G, Schanz H and Whitney R S 2002 *Phys. Rev. Lett.* **88** 104101
Richter K and Sieber M 2002 *Phys. Rev. Lett.* **89** 206801
Turek M and Richter K 2003 *J. Phys. A: Math. Gen.* **36** L455
Spehner D 2003 *J. Phys. A: Math. Gen.* **36** 7269
Müller S 2003 *Eur. Phys. J.* B **34** 305
Müller S, Heusler S, Braun P, Haake F and Altland A 2004 *Phys. Rev. Lett.* **93** 014103
Turek M, Spehner D, Müller S and Richter K 2005 *Phys. Rev.* E **71** 016210
[11] Gutzwiller M C 1990 *Chaos in Classical and Quantum Mechanics* (New York: Springer)
[12] Brack M and Bhaduri R 2003 *Semiclassical Physics* (Boulder: Westview Press)
[13] Berry M V, Keating J P and Prado S 1998 *J. Phys. A: Math. Gen.* **31** L245
[14] Berry M V, Keating J P and Schomerus H 2000 *Proc. R. Soc.* A **456** 1659
[15] Keating J P, Prado S D and Sieber M 2005 *Phys. Rev.* B **72** 245334
[16] Bohigas O, Tomsovic S and Ullmo D 1993 *Phys. Rep.* **223** 43
[17] Eckhardt B, Hose G and Pollack B 1989 *Phys. Rev.* A **39** 3776
[18] Brack M, Mehta M and Tanaka K 2001 *J. Phys. A: Math. Gen.* **34** 8199
[19] Brack M, Fedotkin S, Magner A and Mehta M 2003 *J. Phys.: Condens. Matter* A **36** 1095

[20] Eriksson A B and Dahlqvist P 1993 *Phys. Rev.* E **47** 1002
[21] Yoshida H 1984 *Celest. Mech.* **32** 73
[22] Pullen R A and Edmonds A R 1981 *J. Phys. A: Math. Gen.* **14** L477
[23] Gutzwiller M C 1971 *J. Math. Phys.* **12** 343
[24] de Almeida A M Ozorio and Hannay J H 1987 *J. Phys. A: Math. Gen.* **20** 5873
[25] Sieber M 1996 *J. Phys. A: Math. Gen.* **29** 4715
Schomerus H and Sieber M 1997 *J. Phys.: Condens. Matter* A **30** 4537
Sieber M and Schomerus H 1998 *J. Phys. A: Math. Gen.* **31** 165
[26] Strutinsky V M 1975 *Nukleonika (Poland)* **20** 679
Strutinsky V M and Magner A G 1976 *Sov. J. Part. Nucl.* **7** 138 (*Elem. Part. Nucl.* **7** 356 (1976))
[27] Berry M and Tabor M 1976 *Proc. R. Soc.* A **349** 101
Berry M and Tabor M 1977 *J. Phys. A: Math. Gen.* **10** 371
[28] Creagh S C and Littlejohn R G 1991 *Phys. Rev.* A **44** 836
Creagh S C and Littlejohn R G 1992 *J. Phys. A: Math. Gen.* **25** 1643
[29] Robbins J 1989 *Phys. Rev.* A **40** 2128
[30] Lauritzen B 1991 *Phys. Rev.* A **43** 603
[31] Creagh S C 1993 *J. Phys. A: Math. Gen.* **26** 95
[32] Sadovskii D A and Zhilinskii B 1999 *Phys. Lett.* A **256** 235
Dullin H, Giacobbe A and Cushman R 2004 *Physica* D **190** 15
[33] Keller J B and Rubinow S I 1960 *Ann. Phys.* **9** 24
[34] See, e.g., Wong R 1989 *Asymptotic Approximation of Integrals* (San Diego: Academic Press)
[35] Robbins J 2006 private communication
[36] Sugita A 2001 *Ann. Phys., NY* **288** 277
[37] Creagh S C, Robbins J M and Littlejohn R G 1990 *Phys. Rev.* A **42** 1907
[38] Dyson F and Mehta M 1963 *J. Math. Phys.* **4** 701
[39] Berry M V and Robnik M 1984 *J. Phys. A: Math. Gen.* **17** 2413
[40] Seligman T and Verbaarschot J 1985 *J. Phys. A: Math. Gen.* **18** 2227
[41] Berry M V and Robnik M 1984 *J. Phys. A: Math. Gen.* **17** 2413
[42] Amann Ch and Brack M 2002 *J. Phys. A: Math. Gen.* **35** 6009